Expanding the RGB Color Gamut by the Fourth and Fifth Color

Abstract

The natural world perceived by the human eye cannot be fully represented by light-emitting diode (LED) displays, primarily because natural light sources, such as sunlight, typically have a continuous spectrum covering a wide range of wavelengths from ultraviolet to infrared. In contrast, LED displays typically rely on red, green, and blue (RGB) LEDs combined using the additive color principle to produce visible light. These LEDs emit discrete narrowband spectra, resulting in a limited color gamut, a color range that a system can present. This gamut is often constrained to follow specific standards such as standard RGB (sRGB), AdobeRGB, or DCI-P3, which fail to encompass the full range of colors found in nature. For instance, some deep blues or vivid greens cannot be accurately reproduced on standard displays. In this project, we propose extending the display color gamut by adding a new color to LED displays' commonly used RGB. To achieve this, we utilized calculations to model the response of human cone cells, photoreceptors responsible for color perception, to various wavelengths of light. Through linear combinations, we compared the range of human-visible colors with the RGB gamut. Our calculations revealed that, without considering brightness effects, RGB LED displays can only reproduce approximately 58% of the colors within the human-visible spectrum. By examining the entire visible light spectrum, we identified the optimal additional wavelengths for expanding the LED gamut: 400 nm violet and 680 nm crimson. This crimson, RGB, and violet (CRGBV) system increases the RGB color gamut by around 48%, enabling the present of approximately 86% of the colors visible to the human eye. In practical applications, a circuit system with a Digital to analog converter **(**DAC) and NPN transistors were built to control the current through LEDs. Additionally, a 3D printed mixer, a tube with lens and diffuser, and fibers were used to mix the LEDs.

Introduction

Throughout the history of humanity's efforts to represent the colors of the natural world using electronic devices, continuous technological advancements have significantly transformed the way colors are perceived and expressed. However, it is still not possible to display all the colors that humans can perceive in nature on the monitors. The fundamental reason lies in the biological mechanism of human color perception. Humans perceive color through the cone cells, short-wavelength cone cells (S-cones), medium-wavelength cone cells (M-cones), and long-wavelength cone cells (L-cones), in the retina. Cones have different responses (Fig. 1) to light of different wavelengths. In nature, a continuous spectrum, such as sunlight, stimulates cones across all possible combinations, producing the rich variety of colors humans can perceive. However, electronic displays rely on combinations of usually red, green, and blue (RGB) LEDs to reproduce colors. This approach, based on the principle of additive color, provides only a limited subset of the responses that cone cells can generate, restricting the range of colors monitors can display.

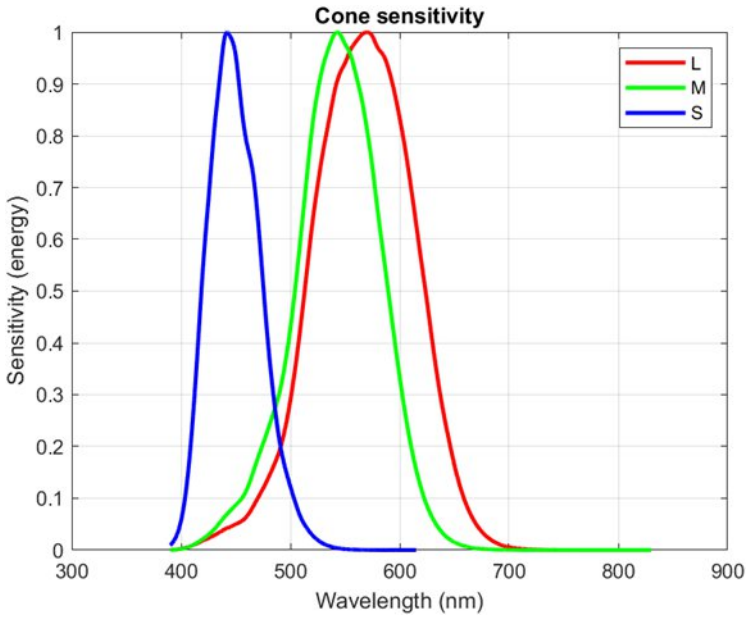

Fig. 1. The responses of L-cones, M-cones, and S-cones to light with different wavelengths. The *x*-axis represents the light wavelength, and the *y*-axis is the normalized cones' responses.

These limitations in replicating natural colors did not deter technological innovation. In the early 20th century, black-and-white televisions [1, 2], the first generation of electronic displays,

presented visual information solely through brightness contrasts. While this technology ushered in a new era of visual entertainment, it fell short of satisfying the human desire for a faithful reproduction of the colorful world. The subsequent advent of color television [2, 3] marked a significant milestone, utilizing the three primary colors, RGB, to synthesize and reproduce colors, allowing electronic devices to render visuals closer to reality for the first time. With the advancement of technology, the sRGB color space [4, 5, 6] emerged as the dominant standard for display devices. Despite its significant advantages in terms of cost and compatibility, sRGB's color gamut remains limited, covering only a fraction of the visible spectrum perceived by the human eye. To address this limitation, subsequent developments introduced wider-gamut standards such as Adobe RGB [6, 7], ProPhoto RGB [6, 8], and DCI-P3 [9] because the LEDs they used have different wavelengths. These expanded gamut standards greatly enhanced the color performance of electronic devices, driving transformations in industries such as photography, cinema, and design. However, even the most advanced wide-gamut display technologies still fall short of covering the entirety of human-visible colors, particularly in rendering certain extreme hues such as deep purples or saturated greens [10].

Against this backdrop, this project aims to explore methods for further expanding the color gamut by proposing a novel five-primary LED system. Traditional three-primary LED systems synthesize colors using RGB light sources, but their gamut is constrained by the spectral response of the cone cells to these three wavelengths. To overcome this limitation, we propose adding a violet and a crimson LED to the existing RGB system to cover shorter wavelengths in the violet and red region, significantly expanding the color gamut. This design optimizes the spectral response to the short-wavelength cone cells (S-cones) and long-wavelength cone cells (L-cones), enabling display devices to reproduce a wider variety of natural colors.

The objective of this study is to design, implement, and validate the performance of the five-primary LED system. We will review the technical history and challenges of color gamut expansion, analyze the theoretical improvements in color coverage offered by the five -primary approach, and evaluate its practical performance through experiments. This breakthrough would not only advances display technology but also provides novel solutions for applications requiring high color fidelity, such as medical imaging, art restoration, and premium displays. Ultimately, it

drives progress in color science and display technology, pushing the boundaries of what is visually achievable.

Method

Brightness Normalization

To facilitate comparison and color gamut size comparison, brightness and chromaticity are separated in this study. For light source *i*, the sum of the responses of the three types of cone cells, $L_i + M_i + S_i$, is considered the brightness, while the ratio of the responses of the three cone cells represents chromaticity. For example, (0.3, 0.1, 0.8) and (0.7, 0.2, 0.3) have the same brightness (since the sum of the three cone responses is 1.2), while (0.2, 0.4, 0.8) and (0.1, 0.2, 0.4) have the same chromaticity (since the ratio of the three cone responses is 1: 2: 4). In this project, we normalize brightness to 1 and only consider the chromaticity, i.e.,

$$\begin{cases} l_i = \dfrac{L_i}{L_i + M_i + S_i} \\ m_i = \dfrac{M_i}{L_i + M_i + S_i} \\ s_i = \dfrac{S_i}{L_i + M_i + S_i} \end{cases} \#(1)$$

in which l_i, m_i, s_i are the response values of the three types of cone cells to light source *i* after brightness normalization.

Additive Color Theory

According to the additive color theory [23], when *n* light sources are combined, the response values of the three types of cone cells are the sum of the response values of the corresponding cones for each individual light. That is,

$$\begin{cases} L = \sum_{i=1}^{n} L_i I_i \\ M = \sum_{i=1}^{n} M_i I_i \\ S = \sum_{i=1}^{n} S_i I_i \end{cases} \#(2)$$

in which, I_i is the relative intensity of light source *i*.

Visual Cone Sensitivity

In this project, we directly used the research results from Colour & Vision Research Laboratory (CVRL) database [11, 12, 24]. CVRL provides the sensitivity of LMS to monochromatic light wavelengths ranging from 390.0 nm to 830.0 nm with a step size of 0.1 nm, and their experiments will be mentioned below briefly. To ensure data reliability, we removed the data at 390-400 nm and 700-830 nm, which means we restrict ourselves to 400-700 nm.

LED Cone Response

Due to the manufacturing process, the LED light sources are discrete, narrow-band spectral emitters, so we cannot directly obtain the corresponding human three-cone cell response values from the database mentioned earlier. Based on the principle of additive color mixing, we applied a calculus-based method to compute the corresponding responses of the human three-cone cells for each LED light source, using the measured spectral distribution (Fig. 2) obtained from the spectrometer [19], with an integration step size of 0.1 nm.

$$\begin{cases} L_{LED} = \int_{\lambda_1}^{\lambda_2} L(\lambda) I(\lambda) d\lambda \\ M_{LED} = \int_{\lambda_1}^{\lambda_2} M(\lambda) I(\lambda) d\lambda \# (3) \\ S_{LED} = \int_{\lambda_1}^{\lambda_2} S(\lambda) I(\lambda) d\lambda \end{cases}$$

In which, $I(\lambda)$ is the relative luminous intensity function of LED. In actual calculations, we take $d\lambda$ as 0.1 nm, λ_1 and λ_2 are taken at 60 nm to the left and right of the peak wavelength respectively.

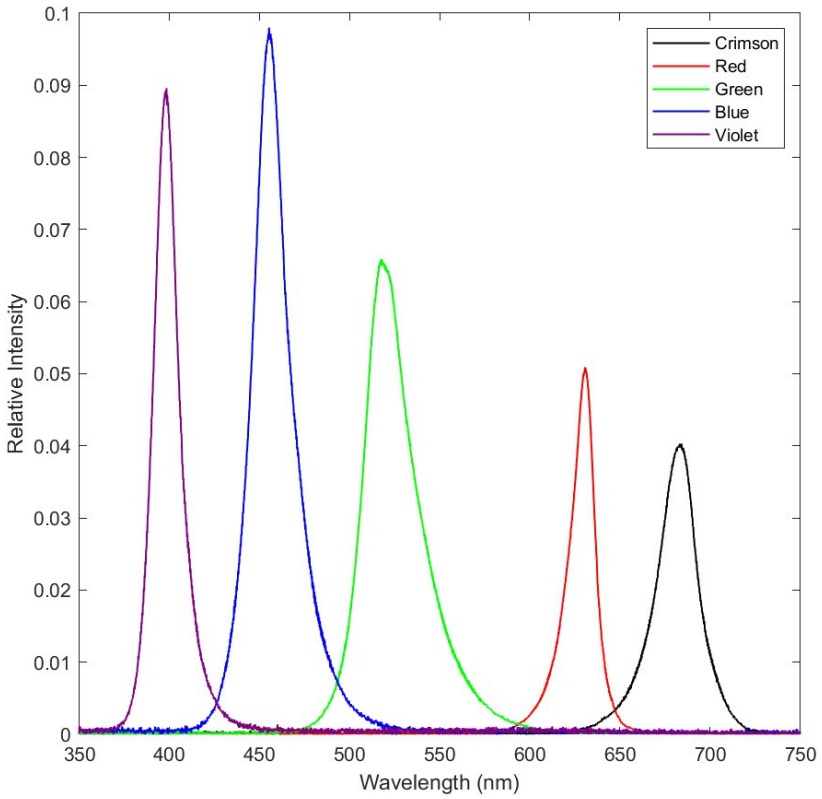

Fig. 2. Distributions of the five CRGBV light sources measured using the spectrometer.

	Peak wavelength (nm)
Crimson	684
Red	630
Green	516
Blue	455
Violet	398

Tab. 2. Data used in the theoretical calculation part.

It can be calculated that under normalized brightness, the three cone cell response values of CRGBV LEDs are

	l	*m*	*s*
Crimson	0.9180	0.0820	0
Red	0.8227	0.1773	0
Green	0.4281	0.5356	0.0363
Blue	0.0598	0.1053	0.8349
Violet	0.0252	0.0304	0.9443

Tab. 3. Under brightness normalization, the three cone cell response values of the CRGBV LEDs used in the experiment.

Color Gamut

According to the principle of additive color mixing and simple linear algebra, we know that under normalized brightness (in the [1, 1, 1] plane), all the colors formed by any combination of light sources are represented by the convex polygonal shape enclosed by these sources in the plane (Fig. 2). For example, the RGB color gamut forms a triangle, the four-color LED gamut forms a quadrilateral, and the visible color gamut is the area enclosed by all visible monochromatic light.

$$\begin{cases} l = \dfrac{\sum_{i=1}^{n} l_i I_i}{I} \\ m = \dfrac{\sum_{i=1}^{n} m_i I_i}{I} \\ s = \dfrac{\sum_{i=1}^{n} s_i I_i}{I} \end{cases} \#(4)$$

In which,

$$I = \sum_{i=1}^{n} I_i \text{ and } I_i > 0$$

Thus,

$$l + m + s = \frac{\sum_{i=1}^{n} \left(l_i + m_i + s_i\right) I_i}{I} = 1 \#(5)$$

Coloring

To display the color gamut more intuitively, we find different sRGB values for the responses of different cone cells and color the corresponding points. We convert LMS to sRGB values through matrix transformations [10] from CIE standards.

$$\begin{bmatrix} X \\ Y \\ Z \end{bmatrix} = \begin{bmatrix} 1.91020 & -1.11212 & 0.20191 \\ 0.37095 & 0.62805 & 0.00000 \\ 0.00000 & 0.00000 & 1.00000 \end{bmatrix} \begin{bmatrix} L \\ M \\ S \end{bmatrix} \#(6)$$

$$\begin{bmatrix} X \\ Y \\ Z \end{bmatrix} = \begin{bmatrix} 0.49000 & 0.31000 & 0.20000 \\ 0.17697 & 0.81240 & 0.01063 \\ 0.00000 & 0.01000 & 0.99000 \end{bmatrix} \begin{bmatrix} R \\ G \\ B \end{bmatrix} \#(7)$$

Here, X, Y, and Z represent the tristimulus values in the CIE 1931 color space, which correspond to the weighted responses of the human visual system to the spectrum of visible light.

Finally, the RGB values usually need to be clipped so that the results fall within the range [0, 1]. Specifically, we set the value of R, G, or B to 0 if it is less than 0 and to 1 if it is greater than 1.

NPN Transmitter

The NPN transistor is composed of three layers of semiconductor device: the emitter (E), base (B), and collector (C) [22]. In an NPN transistor, current flows from C, is regulated through B, and then exits through E.

When a small current flows from B to E, it causes a large current to flow through C to B, thereby generating a larger current to E. The ratio of C current to B current is usually referred to as the transmitter's current gain (β) typically ranging from tens to hundreds, which is 50 in the NPN we are using. The relationship among the currents over B, C, and E can be expressed by the following equation:

$$I_C = \beta I_B \#(7)$$

$$I_E = I_B + I_C \approx I_C \#(8)$$

In which, I_C is the collector current, I_B is the base current, I_E is the emitter current, and β is the current amplification factor of the transmitter.

Result

Theory and Calculation

To quantify and analyze the range of colors perceivable by the human eye and the proportion of these colors that the existing RGB gamut can simulate, we constructed a three-dimensional coordinate system with *L*, *M*, and *S* as the axes. This system represents the human-visible color gamut based on the relationship between light wavelengths and the responses of L-cones, M-cones, and S-cones (LMS) [11, 12], and it was used to compare the distribution of the different color gamuts. Specifically, we utilized wavelength data from ultra-bright 5 mm LEDs provided by Adafruit, with peak wavelengths of 455 nm (blue) [13], 516 nm (green) [14], and 630 nm (red) [15], which correspond to the principal colors in the RGB gamut.

To facilitate comparison, we normalized the luminance of all data points and projected them onto the $L + M + S = 1$ plane, as constant brightness. This approach is similar to the representation method used in the Commission Internationale de l'Éclairage (CIE) chromaticity diagram [10], making it easier to compare the size and coverage of different gamuts intuitively.

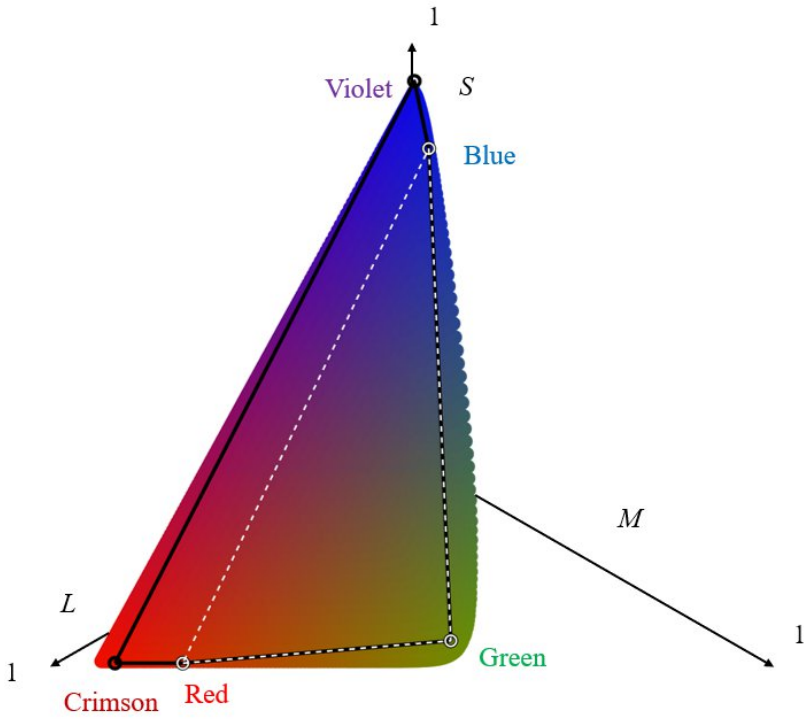

Fig. 3. The colored area represents the human-visible color gamut; the white dot boundary encloses the RGB gamut; the black boundary encloses the CRGBV gamut. The *L*-axis, *M*-axis, and *S*-axis represent the normalized responses of L-cones, M-cones, and S-cones, respectively. Crimson, Red, Green, Blue, and Violet refers to the LEDs used.

Based on Fig.3, we can intuitively observe that the color gamut formed by the RGB primaries occupies only a portion of the area encompassed by the human-visible spectrum. According to calculations, this amount is approximately 58%. Given that the human-visible color gamut significantly exceeds the RGB gamut, we conclude that there is considerable potential for improvement in color simulation by expanding the RGB gamut to include more colors perceivable by the human eye.

To further explore the possibility of gamut expansion, we considered increasing the gamut range by introducing a fourth primary color. To quantify the effect of this expansion, we systematically traversed the visible spectrum from the shortest to the longest wavelength, using each monochromatic light wavelength as the fourth primary color in combination with the RGB primaries. By calculating the area of the color gamut formed by the four primaries, we compared it to the area of the RGB gamut. Specifically, we defined a ratio p to represent the proportion of the four-primary color gamut area relative to the RGB gamut area. This ratio provides a measure of the effectiveness of gamut expansion by introducing another primary color.

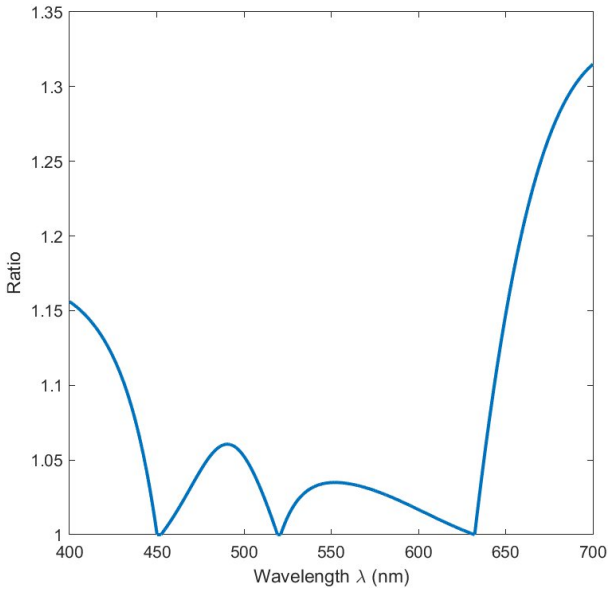

Fig. 4. The x-axis represents the wavelength, and the y-axis represents the ratio of color gamut. The curve represents the ratio of the four-color gamut area to the RGB color gamut area.

In Fig. 4, we observe that at the wavelengths of 455 nm, 516 nm, and 630 nm, p equals 1, indicating that the color gamut area does not expand at these wavelengths. Since these wavelengths correspond to the three RGB primary colors, the fourth primary color overlaps with

these colors and the color gamut area does not increase. This is the expected result of our theoretical calculation. Through this validation step, we initially determined the accuracy of the program. Additionally, we found that *p* reaches a local maximum at approximately 400 nm (in the violet range), 490 nm (in the green range), and 700 nm (in the deep red range). The color gamut area enclosed by the four primaries shows a significant increase compared to the RGB gamut area, particularly at 400 and 700 nm. Therefore, we decided to select a crimson and violet LED as the fourth and fifth primary color for the experiment to extend the color gamut further.

In practice, we chose the 684 nm crimson 5 mm LED and 398 nm violet 5 mm LED [16] as the fourth and fifth primary color. This choice resulted in a 48% increase in the color gamut area compared to the color gamut formed by the RGB primaries alone, representing approximately 86% of the human-visible spectrum, while the RGB gamut only covers around 58%. This result demonstrates that introducing a crimson and a violet LED can significantly expand the color gamut, especially in the deep red and violet light region, allowing the five-primary color combination to simulate colors that are not achievable with the RGB gamut.

Application

Through the analysis and calculations conducted in this study, we conclude that using a crimson and a violet LED as the fourth and the fifth primary color can significantly extend the RGB color gamut, especially in the deep red and violet light region. The combination of five primary colors can cover more visible colors, approaching the actual color gamut range perceived by the human eye. Therefore, we designed a circuit to verify theoretical findings experimentally.

To precisely control the brightness of the LEDs in the experiment, this study utilizes the Adafruit Grand Central M4 [17], the LEDs, a DAC [18], NPN transistors [19], and fixed resistors [20], forming the circuit as Fig. 5.

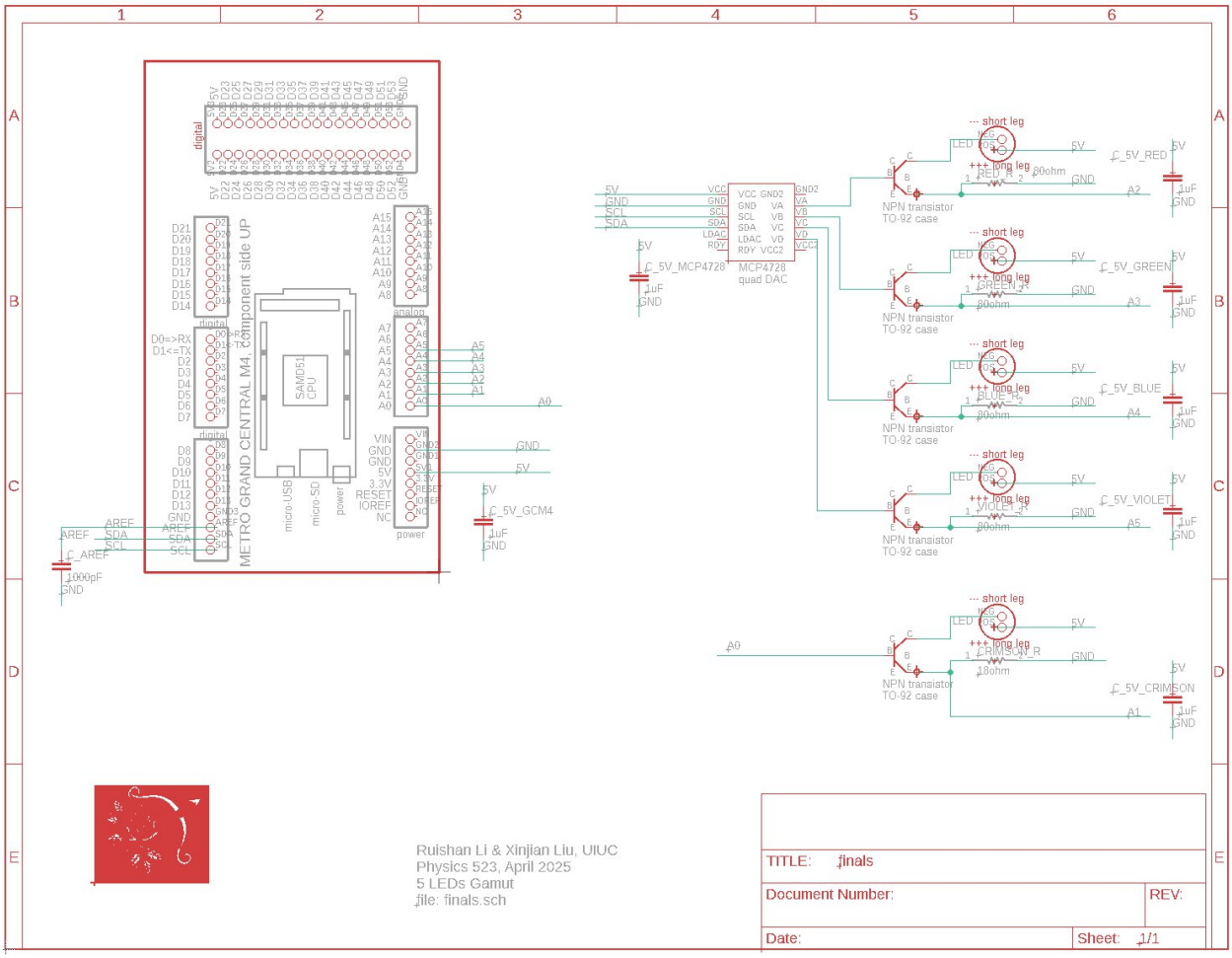

Fig. 5. Circuit schematic diagram.

Notably, LEDs exhibit significant nonlinear working characteristics [21] when they are connected to the circuit individually. When the forward voltage of the LED approaches its threshold voltage, it enters a nonlinear working region, where the current-voltage relationship becomes steeply exponential. A small change in voltage results in a substantial increase in current due to the voltage clamping effect. Therefore, we introduce an NPN transistor into the circuit. By adjusting the base voltage using DAC and placing a resistor at the emitter to limit the current, we can precisely control the current through LEDs while also protecting it from excessive current [22]. This allows the system to precisely control the brightness of the LED within its normal operating voltage range. Additionally, we determined appropriate resistor values through calculation and experimentation to ensure that the current through each LED could approach its maximum rated value while the NPN transistor operates within the active region (Tab. 1 and Fig. 6).

	Range of V_B (V)	Maximum Current (mA)	Resistor (ohm)
Crimson	0.61~1.61	51.38	18
Red	0.61~2.44	20.51	82
Green	0.61~2.44	20.48	82
Blue	0.61~2.44	20.36	82
Violet	0.61~1.46	55.53	13

Tab. 1. Actual data in the circuit measured via the Analog-to-Digital Converter input of Adafruit Grand Central M4. V_B refers to the base voltage of NPN. Maximum Current refers to the maximum current through the LED. Resistor refers to the resistor added at the emitter.

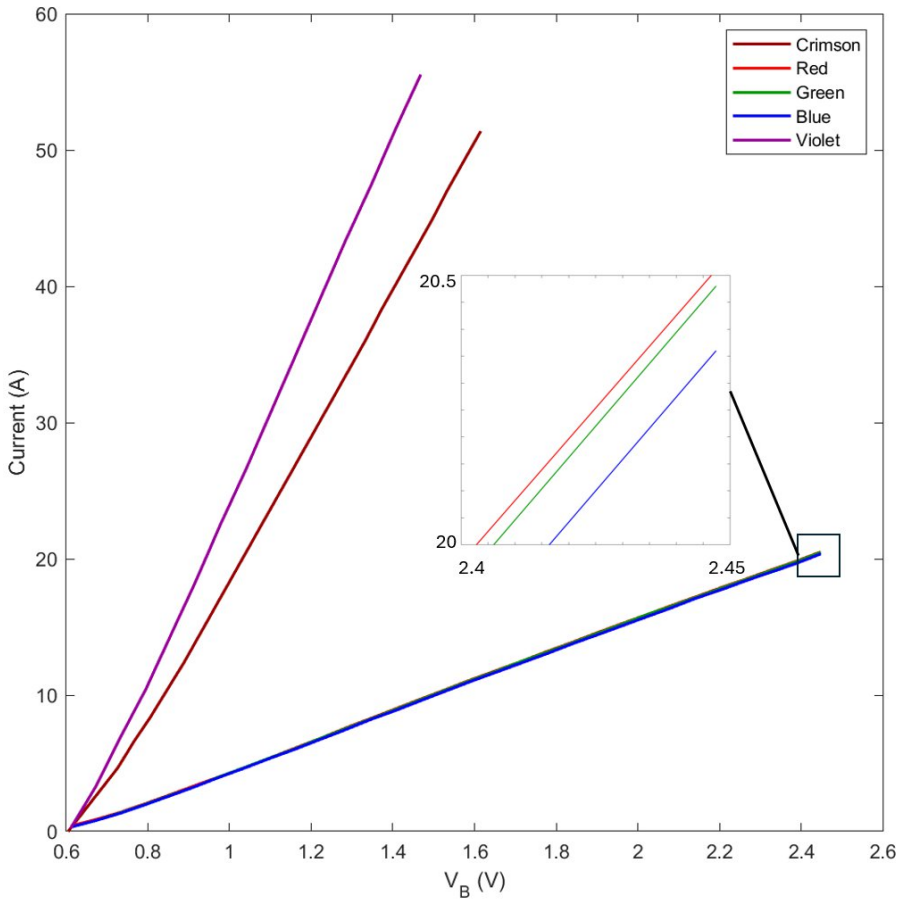

Fig. 6. Actual data in the circuit measured via the Analog-to-Digital Converter input of Adafruit Grand Central M4. The *x*-axis represents V_B, the base voltage of NPN. The left *y*-axis is the current through LEDs. The inset shows a magnified view of the region of V_B = 2.4~2.45 V.

To mix the light sources of different color LEDs, we designed a mix system (Fig. 7) consisting of a 3D printed mixer (Fig. 8), optical fibers, 3D printed LED-to-fiber adapter (Fig. 9), and a tube that contains a lens and a diffuser.

Fig. 7. The mix system. From left to right: PCB board with integrated LEDs; 3D printed LED-to-fiber adapters; optical fibers; 3D printed light mixing tube; another segment of optical fibers; and the final tube.

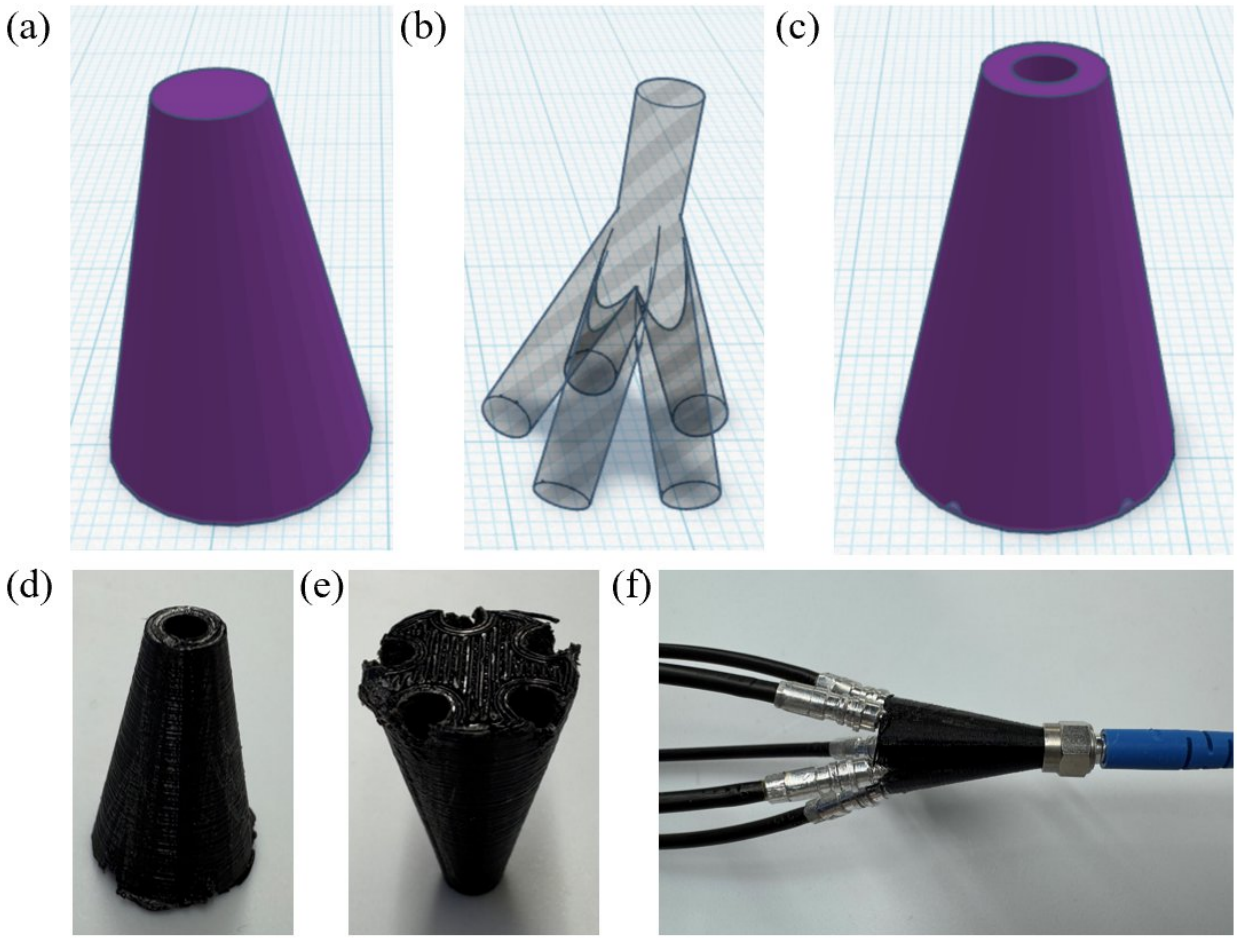

Fig. 8. The mixer. (a) 3D model of the outer shell. (b) Internal channels for multiple fibers. (c) Final combined model integrating both shell and channels into a compact mixing structure. (d) 3D-printed result showing the output channel layout. (e) Top-down view of the mixer showing the input channels layout. (f) The mixer in use. Five input fibers are connected on the left, and the mixed output light is delivered through a single fiber on the right.

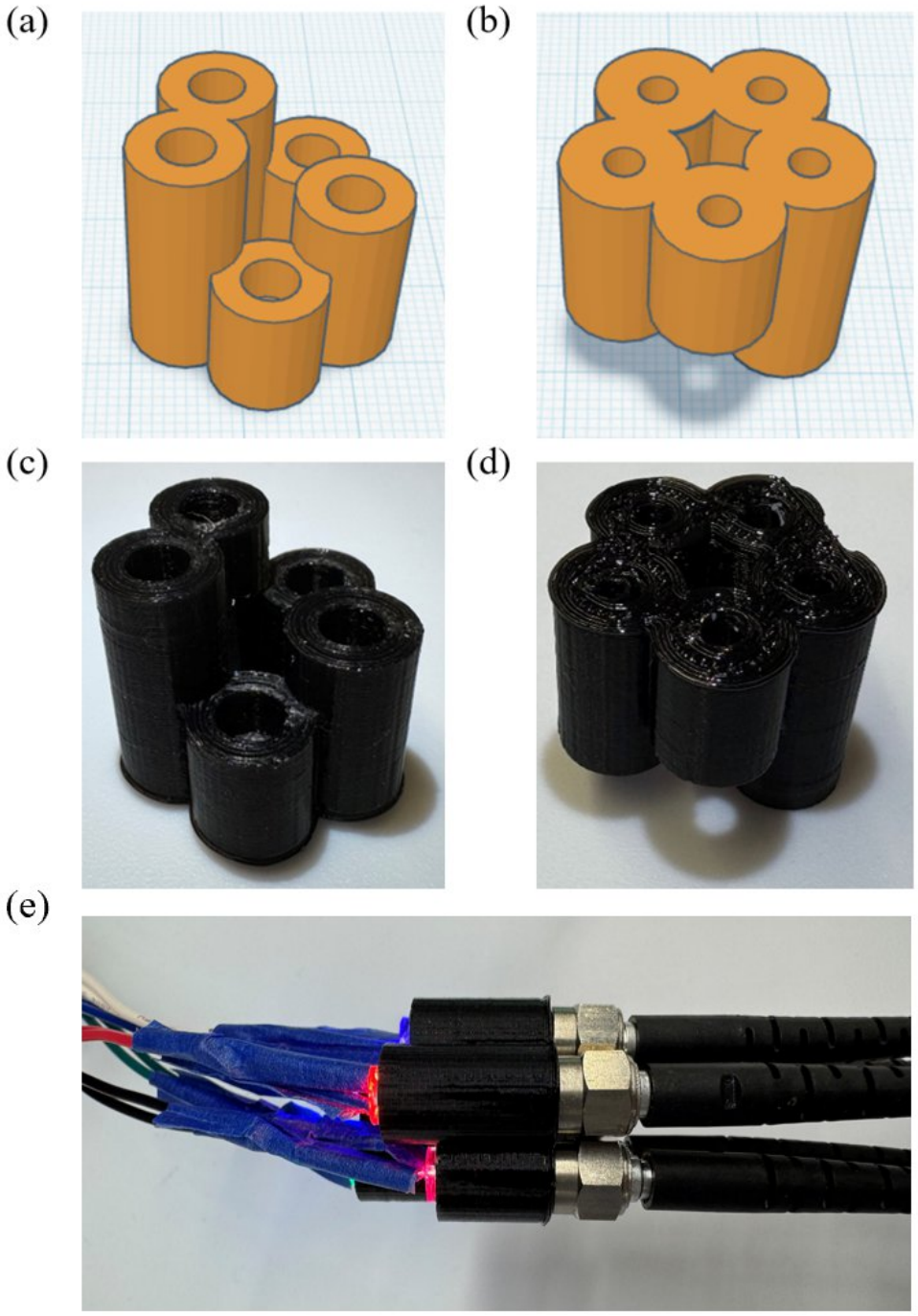

Fig. 9. The LED-to-fiber adapter. (a) 3D model of the adapter with five larger cylindrical channels (for LEDs) arranged symmetrically in the plane but positioned at different heights. (b) Top-down view of the adapter with five smaller cylindrical channels (for fibers) arranged symmetrically. (c) 3D-printed result. (d) Top-down view of 3D-printed result. (e) The adapter in use. The LEDs are positioned on the left side, and the optical fibers are connected on the right.

The channels shown in Fig. 8 are positioned symmetrically to ensure that the five colored lights contribute equally to the output. In contrast, the LED channels shown in Fig. 9 are placed at different heights to compensate for differences in light intensity among the LEDs. Since each color has a different output power, adjusting the height of the channels allows the weaker lights to travel shorter distances, helping to equalize the intensities at the mixing point. This design facilitates a more effective color blending toward the target output.

To verify whether the system mixes the colors uniformly, we measured the spectral composition at different points within the same output light beam (Fig. 10). The results confirm that our system achieves effective color mixing. It is worth noting that although the sampling points showed relatively larger differences at 680 nm, similar variations were also observed when analyzing different sampling points under monochromatic light, suggesting that this deviation may stem from measurement or spatial factors rather than imperfect mixing.

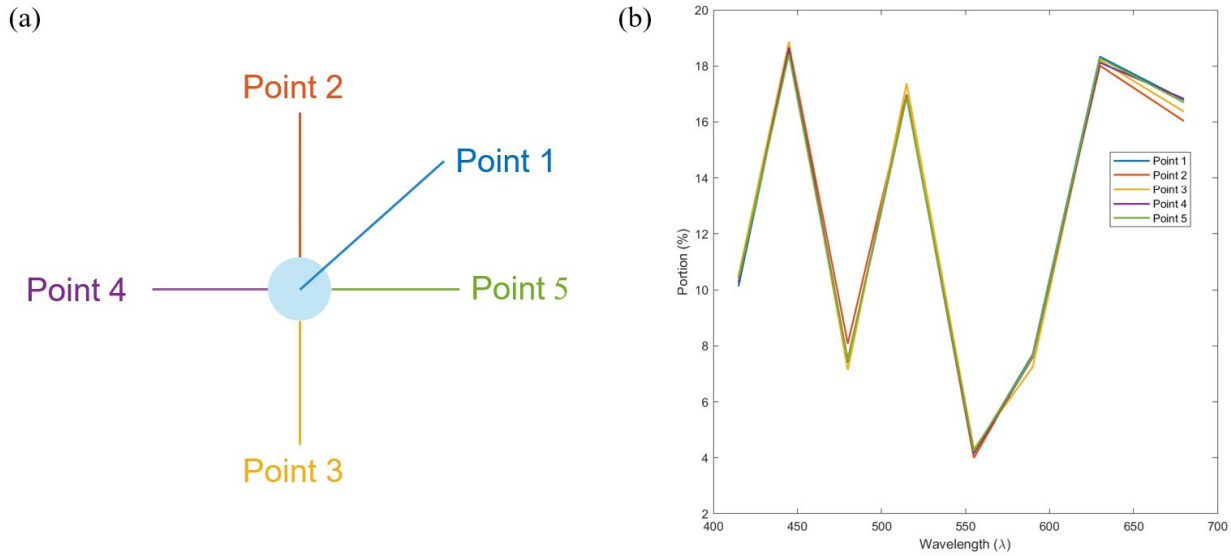

Fig. 10. (a) Four sampling points distributed around the center of the output light spot and one sampling point distributed at the center, used to evaluate the spatial uniformity of color mixing. (b) Spectral composition measured at each point. The high consistency among the five spectra indicates that the mixed light is spatially uniform in terms of color distribution.

Additionally, to further verify the theory and modeling, we implemented the calculated LED intensity ratios in the physical system and observed the resulting output light (Fig. 11), which appeared visually white, consistent with the target color predicted by the model.

Fig. 11. Photograph of the mixed light produced by mixing CRGBV LEDs in the theoretical ratio calculated for white light. The result appears white in practice, confirming the effectiveness of our theory and modeling.

Finally, to demonstrate the ability of the CRGBV gamut to generate colors that are unattainable within the RGB color gamut, we selected a pink target located near the boundary between crimson and violet (Fig. 12). By comparing this point to the closest achievable color within the RGB gamut, a clear perceptual difference can be observed. It is important to note that the nearest RGB color was not determined based on Euclidean distance in the LMS color space, but rather in the CIELAB color space. This is because LMS is not a perceptually uniform color space, whereas CIELAB is designed to reflect perceptual uniformity, meaning that Euclidean distances in CIELAB space more accurately represent perceived color differences. [20].

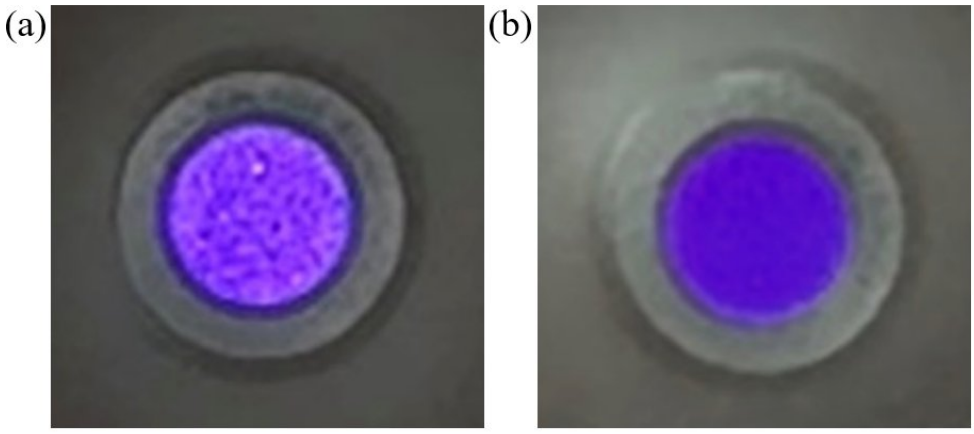

Fig. 12. (a) The pink target located near the boundary between crimson and violet, generated using the CRGBV LED system. (b) The closest achievable color within the standard RGB gamut for comparison. Note: due to limitations of camera sensors and display devices, as well as the fact that the pink target lies outside the RGB gamut, the actual appearance may differ from what is shown. This image is intended for reference only.

Conclusion

This project demonstrates that sRGB LED displays significantly fall short of the full color gamut perceivable by the human eye, covering only about 58%. By introducing a fourth principal color, 400 nm violet LED, we achieved approximately 48% progress over sRGB LED, about 86% of visible gamut.

Theoretical calculations revealed that crimson and violet light are particularly effective in expanding the color gamut, especially within the deep red and violet spectral range. In applications, the project developed a practical circuit system, including CRGBV LEDs, DAC, NPN transistors, and a mix system consisting of a 3D printed mixer, optical fibers, 3D printed LED-to-fiber adapter, and a tube that contains a lens and a diffuser.

To validate the system's capability to produce colors beyond the conventional RGB gamut, we selected a pink target located near the boundary between crimson and violet. Comparing this target to the closest achievable color within the RGB gamut revealed a noticeable perceptual difference. It's important to note that the nearest RGB color was identified based on Euclidean distance in the CIELAB color space, rather than the LMS space. This choice is due to CIELAB's

design for perceptual uniformity, where Euclidean distances correspond more closely to perceived color differences.

This project demonstrates the potential of a five-principal-color LED system for improved color reproduction, which may be useful for practical applications such as medical imaging, design, art restoration, and display technology.

Prospect

Future research can build upon both the theoretical and practical aspects of this project to further enhance color reproduction capabilities.

From a theoretical perspective, the addition of a sixth or even seventh LED, particularly in underrepresented spectral regions such as cyan and yellow, could further expand the color gamut.

On the application side, although the current experiments provide strong visual and qualitative evidence, more rigorous and quantitative evaluation methods are needed to validate system performance. Future work could focus on developing reproducible, standardized measurement techniques, such as spectrophotometric comparison or perceptual color matching tests, to objectively evaluate the color-mixing accuracy and gamut coverage of the CRGBV system.

Additionally, one important goal is to demonstrate, through experiment, that the CRGBV system can simulate colors not achievable by the RGB system. This poses unique challenges due to perceptual variability among individuals, camera and display calibration differences, and the difficulty of visualizing out-of-gamut colors on standard monitors. Addressing these challenges will require methods that bridge psychophysical testing and objective spectral analysis, ensuring results that are both perceptually meaningful and scientifically robust.

Acknowledgements

This project would not have been possible without the guidance and support of many individuals. We would like to sincerely thank Dr. George Gollin for his valuable insights, technical guidance, and resources throughout the project. We also appreciate the support provided by the Dr. Yuk-Tung Liu, Dr. Chad Lantz, and Dr. Chen-Yu Liu, which enabled the design, fabrication, and testing of the system. Special thanks to our classmates who contributed companionship and

encouragement during the development process. We are also deeply grateful to our families for their unwavering emotional support and generous financial assistance, which provided the foundation for us to focus wholeheartedly on our work.

Over the past year, we have overcome many challenges, gained valuable knowledge, and experienced significant personal growth. This project is not only a technical achievement, but also a meaningful milestone in our journey. It will undoubtedly remain a vivid and unforgettable chapter in our lives.

Reference

[1] Whitaker, R. (1973). "The Invention of Television." McGraw-Hill.

[2] Fisher, D., & Fisher, M. (1996). "Tube: The Invention of Television." Random House.

[3] Schure, A. (1955). "Color Television: Theory and Practice." McGraw-Hill

[4] Stokes, M., Anderson, M., Chandrasekar, S., & Motta, R. (1996). "A Standard Default Color Space for the Internet - sRGB." HP and Microsoft.

[5] Poynton, C. (2003). "Digital Video and HDTV: Algorithms and Interfaces."

[6] Sharma, G. (2003). "Digital Color Imaging Handbook."

[7] Adobe Systems Incorporated. (1998). "Adobe RGB (1998) Color Image Encoding."

[8] Kodak Inc. (1999). "ProPhoto RGB Color Space Specification."

[9] Digital Cinema Initiatives, LLC. (2007). "Digital Cinema System Specification v1.0."

[10] CIE. (1931). "Standard Colorimetric System."

[11] Stockman, A., Sharpe, L., & Fach, C. (1999). "The spectral sensitivity of the human short-wavelength sensitive cones derived from thresholds and color matches." Vision Research.

[12] Stockman, A., & Sharpe, L. (2000). "The spectral sensitivities of the middle- and long-wavelength-sensitive cones derived from measurements in observers of known genotype." Vision Research.

[13] Adafruit. "https://www.adafruit.com/product/297".

[14] Adafruit. "https://www.adafruit.com/product/300".

[15] Adafruit. "https://www.adafruit.com/product/301".

[16] Adafruit. "https://www.adafruit.com/product/1793".

[17] Adafruit. " https://www.adafruit.com/product/4084".

[18] Adafruit. "https://www.adafruit.com/product/4470".

[19] "https://www.thorlabs.com/catalogpages/v20/1311.pdf".

[20] International Commission on Illumination (CIE). (1976). Colorimetry (2nd ed.). CIE Publication No. 15.2.

[21] Bhattacharya, P. (1997). "Semiconductor Optoelectronic Devices." Prentice Hall.

[22] Sze, S. M. (2002). "Semiconductor Devices: Physics and Technology." John Wiley & Sons.

[23] Berns, R. S. (2000). "Principles of Color Technology." John Wiley & Sons.

[24] CVRL. "http://cvrl.ucl.ac.uk".

Supplement

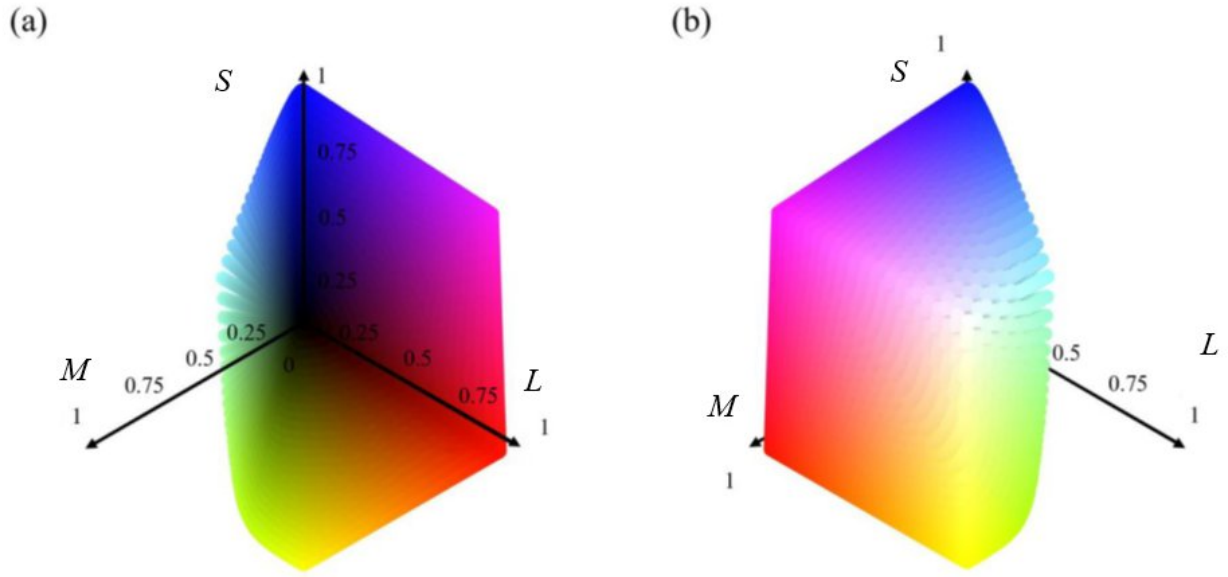

Fig. S1. Different views of three-dimensional human-visible color gamut. (a) the view from direction [-1, -1, -1] and (b) the view from direction [1, 1, 1].

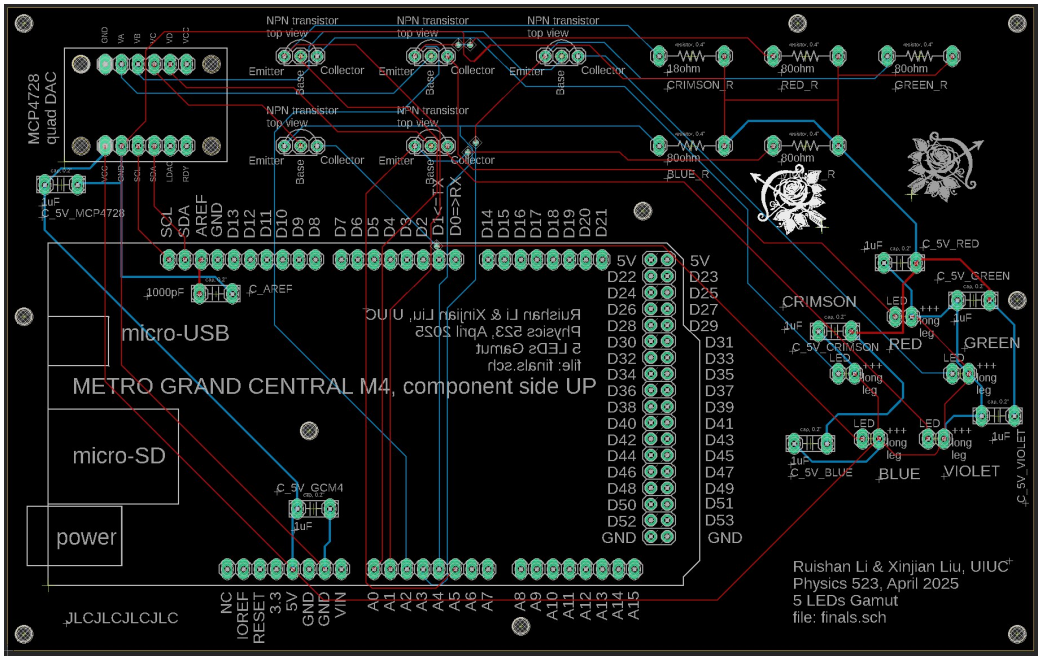

Fig. S2. PCB layout.

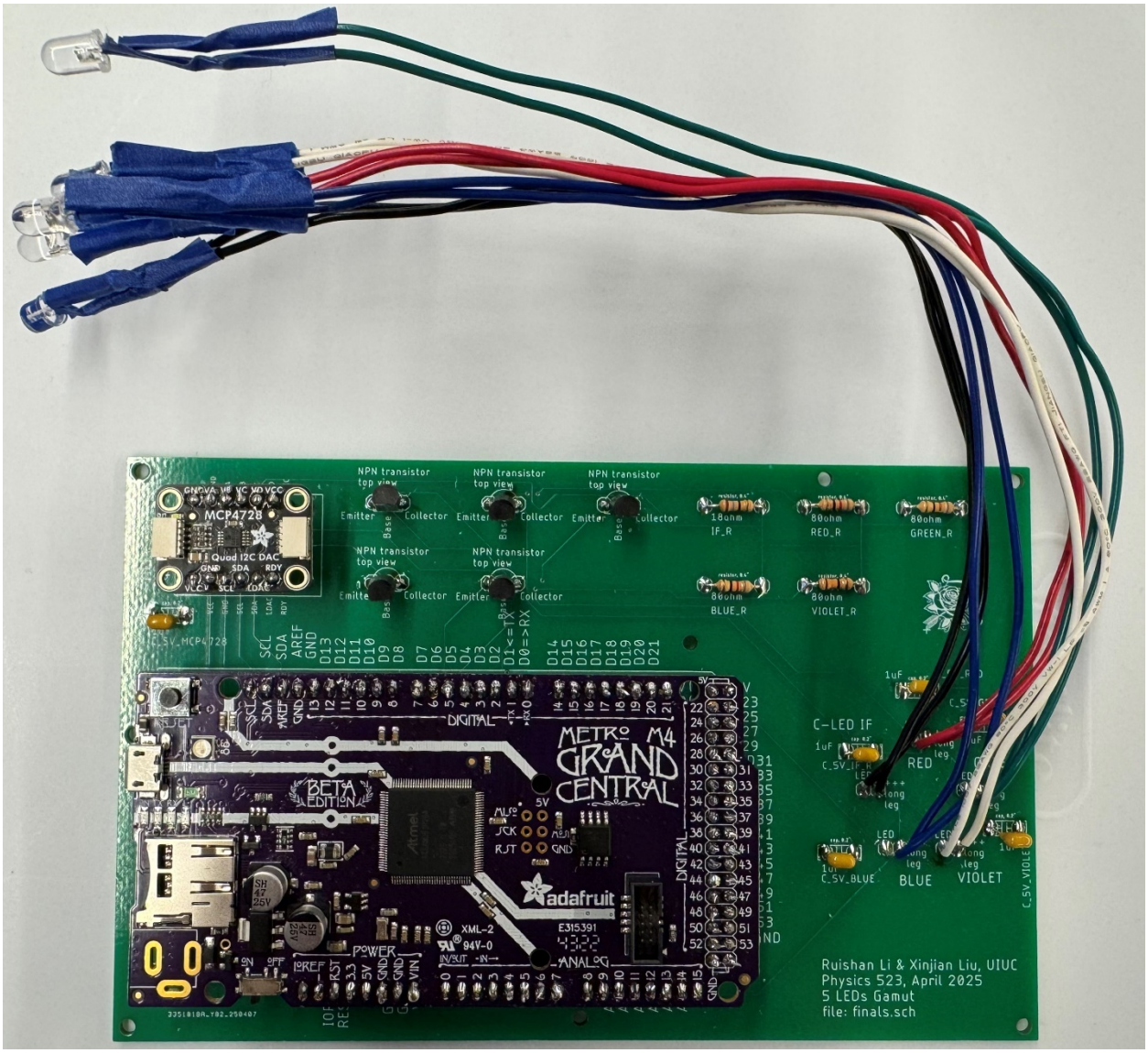

Fig. S3. PCB physical picture.

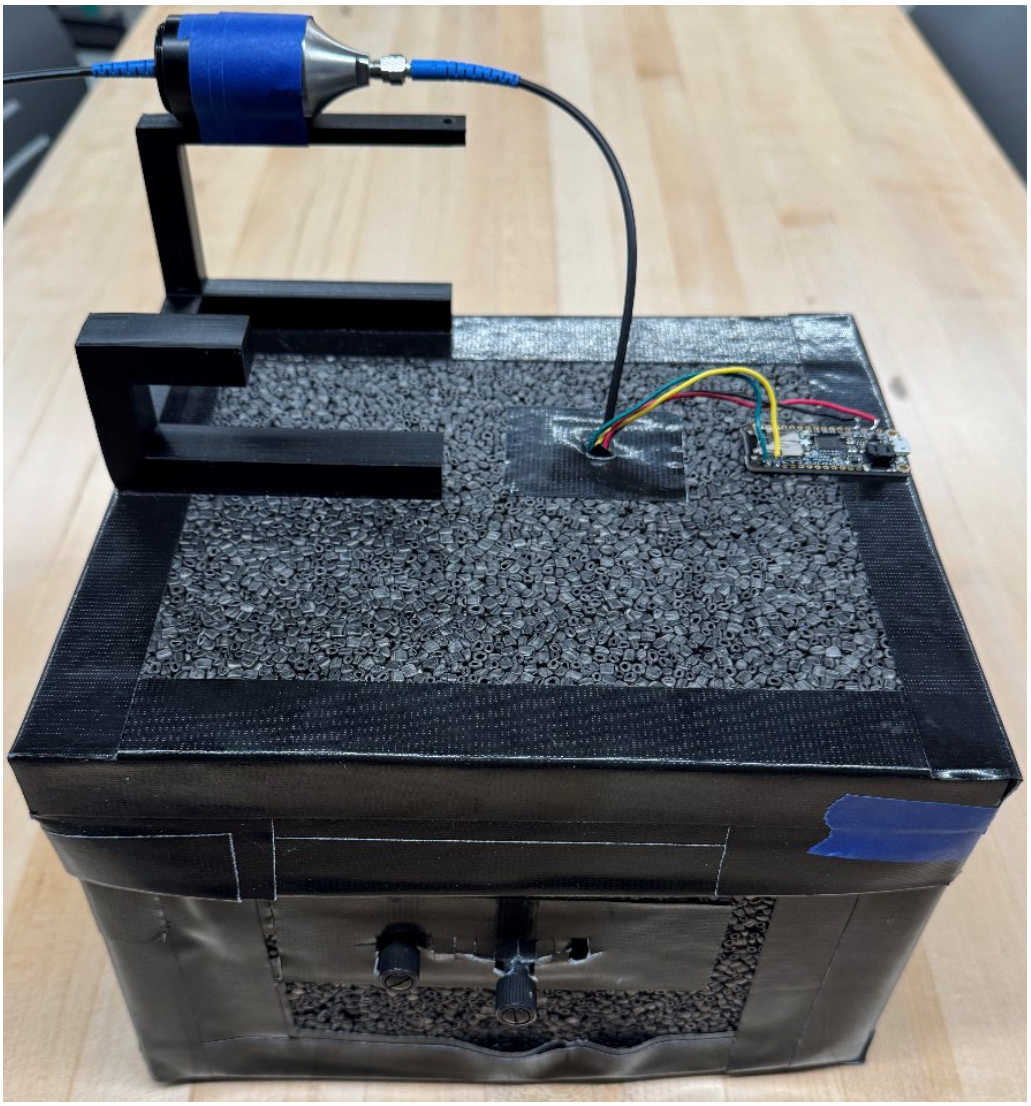

Fig. S4. Dark box designed to measure light spot.

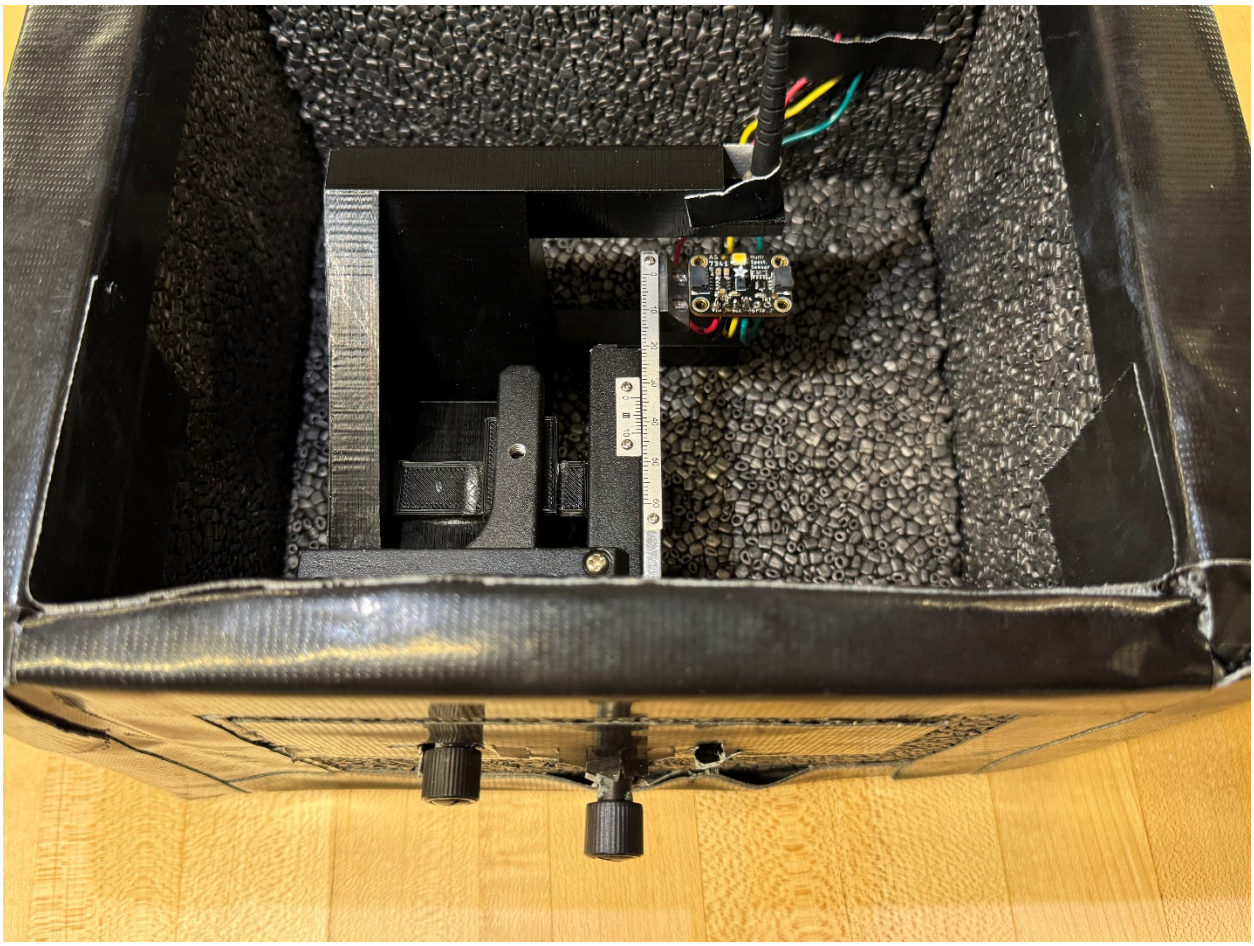

Fig. S5. Inner layout of dark box. Measurement setup for analyzing the spectral composition of the output light spot using the AS7341 10-channel spectral sensor. The sensor is mounted on a horizontally adjustable platform, while two external knobs allow fine-tuning of its horizontal position. To minimize the influence of vibration and ambient light, the entire system is stabilized with a 3D-printed frame and secured using tape.